Civil Engineering Infrastructures Journal, 2026, 59(1): 123-138
DOI: 10.22059/ceij.2024.378792.2088

RESEARCH PAPER

Experimental and Numerical Study of the Effect of Friction Damper on the Seismic Behavior of Concrete Frame

Najafi, S.[1], Aghayari, R.[2*], Cheraghi, K.[1] and TahamouliRoudsari, M.[3]

[1] M.Sc., Department of Civil Engineering, Faculty of Engineering, Razi University, Kermanshah, Iran.
[2] Associate Professor, Department of Civil Engineering, Faculty of Engineering, Razi University, Kermanshah, Iran.
[3] Associate Professor, Department of Civil Engineering, Kermanshah Branch, Islamic Azad University, Kermanshah, Iran.

Received: 1 Jul. 2024; Revised: 31 Aug. 2024; Accepted: 2 Oct. 2024

ABSTRACT: Friction dampers are an effective way to reduce earthquake forces in concrete structures. The study examines the performance of three experimental Reinforced Concrete (RC) moment frames with different friction dampers. Two dampers had a transmission function, and one had a rotational function. After loading, their hysteresis diagrams were extracted and compared. In order to study the impact of slip force on the seismic performance of a concrete frame, numerical analyses were conducted. This section focused on a rotational damper that had demonstrated excellent experimental performance. At first, the friction damper was investigated numerically, and an approximate equation was proposed to calculate its sliding force. Similarly, following validation, the concrete frame equipped with rotational friction dampers was numerically analyzed. The analysis was performed using nonlinear static analysis, and the outputs of the model included resistance, ductility, energy dissipation, and stiffness. The experimental results demonstrated that, in terms of ductility, energy dissipation, and elastic stiffness, the rotational friction damper exhibited the best performance. Based on the numerical results, the best performance of the frame was obtained when the sliding force of the damper was equal to 1.4 times the strength of the bare frame.

Keywords: Concrete Frame, Experimental Test, Friction Damper, Numerical Method, Retrofitting.

1. Introduction

Figures and statistics of earthquake casualties and damage indicate that many methods of dealing with seismic forces should be reconsidered, or more reliable alternative methods should be considered (Permanoon et al., 2024; GanjiMorad et al., 2024). Today, one of the main challenges to achieving this goal is to apply and present new methods in the concepts of seismic design of structures (Roodpeyma and Mahmoudzadeh Kani, 2023; Javaheri-tafti and Hajisafari, 2025; Aydin et al., 2023).

Numerous methods have been proposed to reduce system vibrations (Ozturk et al., 2022). One method that has garnered considerable attention is passive dampers (Aydin et al., 2019). Passive seismic systems absorb and dissipate seismic

* Corresponding author E-mail: reza_agh@razi.ac.ir

energy without external power. Examples include viscous dampers (Hu et al., 2023), yielding dampers (Cheraghi et al., 2024; Cheraghi and TahamouliRoudsari, 2024; Cheraghi et al., 2023), friction dampers (Gao et al., 2023), and base isolators, all designed to enhance earthquake resistance by reducing vibrations and limiting structural damage.

In this study, one of these methods, passive control of structures, is investigated using friction dampers. Due to its simplicity in construction, lack of requirement for expensive materials, and minimal need for specialized labor during installation and commissioning, this damper has been considered a suitable option for research purposes in civil engineering (Liu et al., 2023; Maida and Sakata, 2021; Aghani et al., 2024). Numerous lateral resistance systems have been proposed to strengthen concrete moment frames. One such device is the friction dampers, which have been extensively studied by many researchers.

Bruschi and Quaglini (2022) presented a novel hysteretic friction damper, the prestressed lead damper with straight shaft (PS-LED), designed for seismic rehabilitation of Reinforced Concrete (RC) framed buildings. Characterized by high stiffness, damping capability, compact design, and low manufacturing cost, the PS-LED was experimentally validated and modeled in OpenSees. Numerical investigations on a typical Italian RC frame structure retrofitted with PS-LED, targeting either elastic or partially dissipative behavior, showed satisfactory seismic performance. A comparative analysis with conventional steel hysteretic dampers revealed the superior performance of PS-LED in controlling internal force increases.

Morgen and Kurama (2008) evaluated the seismic response of unbonded post-tensioned precast concrete moment frames with friction dampers. Nonlinear analyses showed dampers enhance energy dissipation while post-tensioning ensures self-centering. The study critically assessed seismic design and compares various reinforcement strategies, highlighting the effectiveness of friction dampers. Morgen and Kurama (2008) described a seismic strengthening technique for moment-resisting frame buildings using a hybrid wall-type damping system combining friction and metallic dampers. Full-scale cyclic tests on a non-ductile RC frame and four strengthened frames showed that the damping system significantly improved maximum strength, stiffness, and energy dissipation despite some discrepancies in predicted stiffness due to anchorage softening.

Huang et al. (2021) investigated the seismic performance of post-tensioned self-centering precast concrete frames with variable friction dampers and hidden corbels. Theoretical and numerical models were developed for the proposed dampers, allowing designs to meet target performance objectives at different seismic hazard levels. Nonlinear time-history analyses for a six-story building showed that frames with the proposed dampers effectively mitigate drift concentration and reduce overall drift demands compared to frames with conventional constant friction devices, meeting the design basis earthquake and maximum considered earthquake objectives.

Kim and An (2016) investigated optimal friction damper distribution in non-seismic RC structures using a genetic algorithm. Nonlinear analyses showed a 30% reduction in maximum roof displacement and a 40% reduction in inter-story drift ratio. The genetic algorithm proved more efficient than intuitive methods, requiring fewer dampers.

Moon et al. (2017) proposed a friction-damping system for seismic retrofitting of old low- to mid-rise RC buildings in seismically active regions. The system included dampers and a braced frame to enhance seismic performance. Their study introduced a design method validated on a six-story RC building originally designed for gravity loads only.

Nabid et al. (2020) discussed the

effectiveness of friction-based dampers as efficient energy dissipation devices, highlighting their adjustability and high energy dissipation capacity. However, they noted that uniform slip load distributions in conventional designs could localize damage. The study developed an energy-based optimization methodology to enhance seismic performance by redistributing slip loads and reducing inter-story drift ratio and global damage in RC frames.

Liu et al. (2023) investigated self-centering walls equipped with slip-friction dampers, emphasizing their simplicity and stable energy dissipation. Experimental results with brass-steel interfaces showed a significant 81.2% increase in energy dissipation and improved post-yield stiffness. The walls sustained 3.0% horizontal drift without major damage and minimal residual drift, facilitating post-earthquake recovery and practical repair ability.

Gao et al. (2023) explored the dynamic performance of metal friction dampers through cyclic loading tests on 30 specimens with various friction pairs. Results demonstrated consistent rigid-plastic hysteresis across loading rates, meeting FEMA-356 standards (FEMA, 2000). Loading rates affected normal force loss and friction coefficients. Recommendations included pre-friction for certain pairs and calibration for others, with established analytical models for dynamic friction coefficients.

In previous studies, it has been observed that translational and rotational friction dampers have not been cyclically tested on concrete frames experimentally or numerically. Therefore, this research initially examines three experimental specimens of RC moment frames equipped with both translational and rotational friction dampers. Based on experimental evidence and model results, it was observed that rotational dampers perform better. Consequently, a numerical model is employed for further studies on this model. Initially, only the friction damper is modeled, and its sliding force is calculated for different conditions. Then, an approximate equation is proposed to estimate the sliding force of this damper based on the curve fitting technique. Finally, the numerical investigation of the effect of the rotational friction damper on the concrete frame is conducted. The sliding force of the friction damper is the variable in the numerical model. Additionally, the model is analyzed nonlinearly and statically, focusing on outputs such as elastic stiffness, strength, energy dissipation, and ductility.

2. Test Setup

In this study, three concrete frames equipped with friction dampers were examined in the laboratory. Figure 1 shows the bare concrete frame and its molding.

(a)

(b)

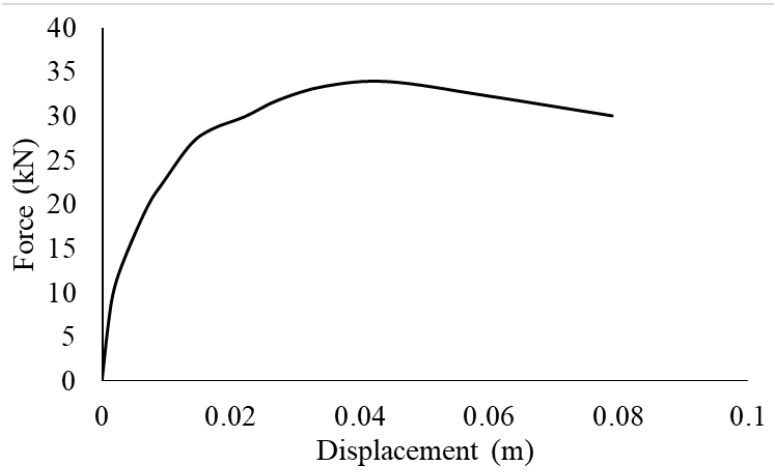

(c)

Fig. 1. a) The reference RC moment resisting frame; b) The steel mold; and c) The backbone diagram (Rahimi et al., 2022)

This frame, at a 1:3 scale, comprises a column with a height of 1 m and a beam with a length of 1.45 m. The dimensions of the beam, column, and foundation sections and their rebar details are presented in Table 1. As shown, the dimensions of the beam and column are considered to be identical. To satisfy the weak beam-strong column criterion, the dimensions of the column reinforcement are designed to be larger than those of the beam. In several previous studies, frames with the same specifications have been equipped with various lateral resistance systems. The concrete pouring for this frame and the foundation was carried out simultaneously. In this study, three different types of friction dampers were utilized for retrofitting a concrete frame structure. The frame used in this study was the same as the one described in the reference (Rahimi et al., 2022).

Note that the experiments in the present study and the references were performed in a short time, and the specifications of concrete frames in both studies were identical. The force-displacement curve of the experimental bare frame is also shown in Figure 1c. The compressive strength of concrete samples was 38.3 MPa. Table 2 presents the specifications of the reinforcements used in the concrete frame, including yield and ultimate stress. This section provides details on friction dampers. These models are M1, M2, and M3, as shown in Figure 2. As observed, models M1 and M2 are designed with translational behavior, whereas model M3 demonstrates rotational behavior. This implies that the frame drift ratio in the translational friction damper only results in its displacement, whereas in the rotational model, the damper members undergo rotation. In Model M2, the damper is connected to the beam using chevron braces. The braces are fixed, and the displacement of the damper and the frame is the same.

Table 1. The dimensions and reinforcement of the beam, the column, and the foundation

Element	Section (mm)	Main bars	Ties and stirrups
Column	150 × 150	4 Φ14	Φ8 @ 45 mm
Beam	150 × 150	4 Φ10	Φ8 @ 45 mm
Foundation	200 × 300	4 Φ 10 top and 3 Φ 14 bottom	Φ8 @ 80-100 mm

Table 2. The stresses derived from the tensile tests of the main steel bars, stirrups, and ties include yield, failure, and ultimate stresses (MPa)

Rebar size	Yield stress	Ultimate stress	Breaking stress
Φ8	420	607	519
Φ10	371	570	523
Φ14	395	610	555

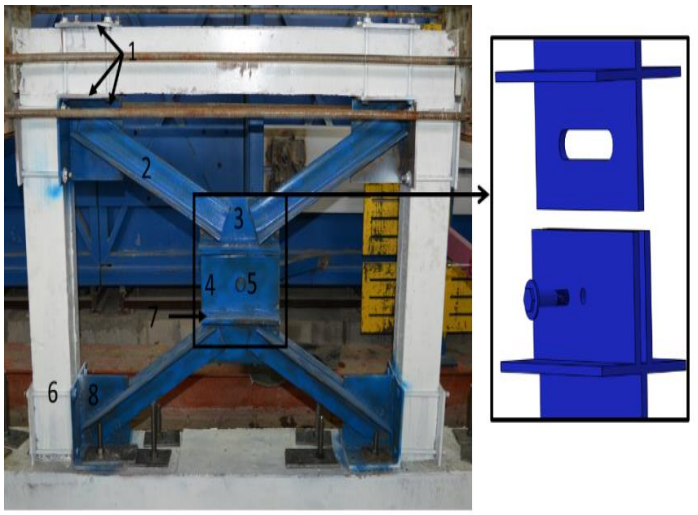

1-PL200x200x10 mm 2-2L80x8 mm 3-PL300x120x10 mm 4-3PL300x150x10 mm
5-4Bolt16 mm Gr8.8 6-4Bolt16mm Gr8.8 7-PL300x150x15 mm

(a)

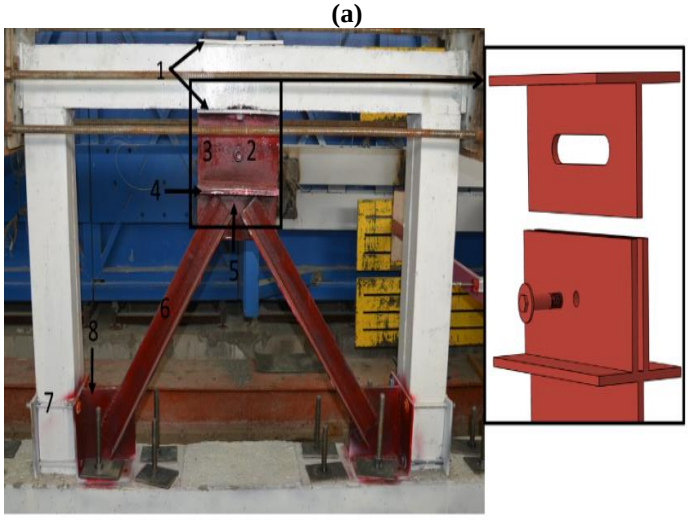

1-PL300x150x10 mm 2-Bolt16mm Gr8.8 3-3PL300x150x10 mm 4-3PL300x150x15 mm
5-PL300x120x10 mm 6-2L80x8 mm 7-4Bolt 14mm Gr8.8 8-PL200x200x10 mm

(b)

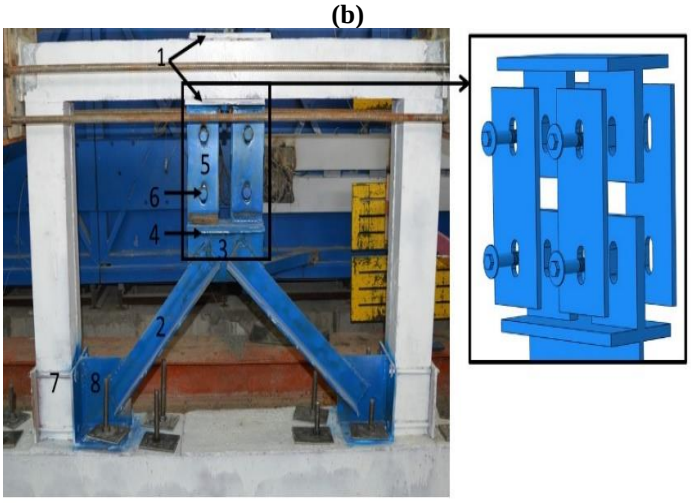

1-PL300x150x10 mm 2-2L80x8 mm 3-PL300x120x10 mm 4-PL300x150x15 mm
5-PL260x120x10 mm 6-4Bolt16mm Gr8.8 7-4Bolt14mm Gr8.8 8-PL200x200x10 mm

(c)

Fig. 2. Details of the experimental examples: a) M1; b) M2; and c) M3

Since preliminary numerical analyses showed that the beam exhibits vertical and horizontal displacement, the damper's plate opening height was considered greater than the diameter of the bolt. In the third model, the damper operates rotationally, with the lower part designed as fixed and its upper displacement equal to the displacement of the frame. Additionally, in this model, the beam exhibits horizontal and vertical displacements, so the height of the holes is designed to be larger than the diameter of the bolts. In this configuration, the damper can be displaced vertically to reduce the vertical force on the beam. Figure 3 shows the experimental test setup.

Twelve 12.9 bolts, according to the British Standards Institution (2009) with a diameter of 26 mm, were connected to the foundation to form a very strong chassis for the experimental floor. In addition, the bolts were prestressed, and two angulars were installed on either side of the foundation to prevent the horizontal slip between the foundation and the chassis. Quasi-static loading was applied by an actuator with a capacity of 1000 kN as tension and pressure on the top of the frames. The type of loading displacement control had a maximum displacement capacity of 150 mm; one end of the actuator was connected articulately at the top of the frame, and the other end was rigidly connected to the reaction frame. The ACI Committee 374.1-05 protocol (ACI Committee 374, 2005) was used for the return protocol (Figure 4). The test was performed on all models with up to 6% drift. Drift ratio values were multiplied by 1 m height (height of the frame from the beam axle to the top of the foundation) and applied as a lateral displacement above the frame. Linear Potentiometer Transducer (LPT) with a precision of 0.01 mm and a maximum displacement capacity of 0.1 and 0.2 m was used to measure displacement at the top of the frame and in the middle of the column. A 32-channel data logger was used to record the information every 10 sec.

The loading speed was applied at a rate of 5 mm/min. At this loading rate, it was ensured that no vibrations were observed in the hysteresis curve. To determine the seismic results of the frame, such as strength, elastic stiffness, and ductility, the backbone diagram of the samples was first drawn until the peak moment and then approximated with a bilinear diagram.

According to the equivalent energy law, a bilinear diagram should be drawn so that the area below it is equal to the backbone (BSSC, 2006). Figure 5 reveals the equivalent two-line qualitative diagram and the backbone. Elastic stiffness and ductility can be defined as Eqs. (1) and (2), respectively.

$$K_{\mathrm{e}} = V_{\mathrm{y}}/D_{\mathrm{y}} \quad (1)$$

$$\mu = D_{\mathrm{u}}/D_{\mathrm{y}} \quad (2)$$

where V_y and D_y : denote the yield strength and the corresponding yield displacement, respectively, while D_u: represents the maximum (ultimate) displacement.

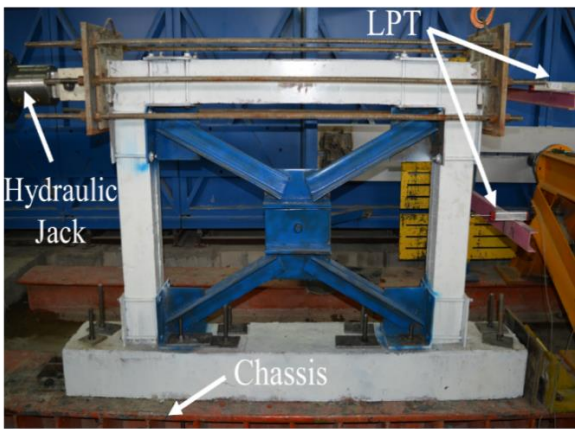

Fig. 3. Test setup

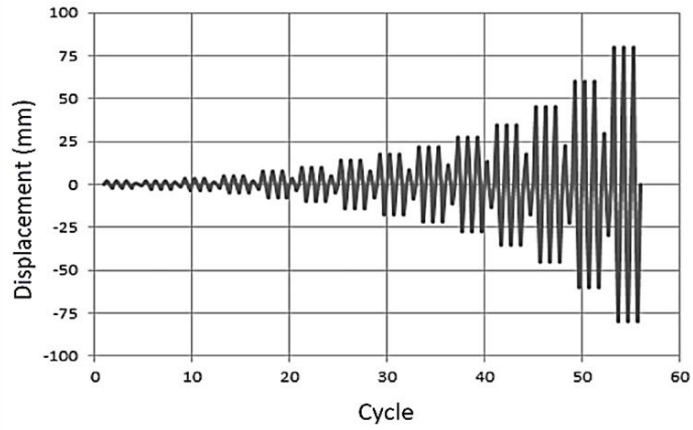

Fig. 4. Loading history based on the ACI committee 374.1-05 standard (ACI Committee 374, 2005)

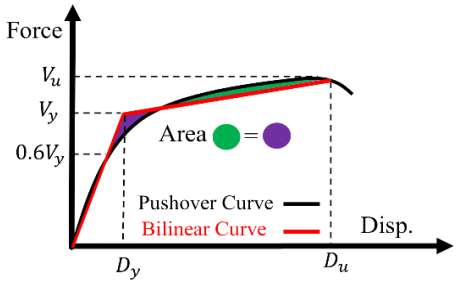

Fig. 5. The backbone and the equivalent bilinear diagram

Figure 6a reveals the hysteresis diagram of the M1 sample. As can be observed, the model has not performed relatively well in terms of energy dissipation, and it has irregular and almost thin rings. The first drop of the diagram occurred at a drift of 0.02, and finally, the loading at a drift of 0.06 ended with the failure of the column. Figure 6b indicates the deformation of the frame at 0.02 drift moment when the first member of the structure, the column, was damaged. Since the column is one of the important members of the structure and must yield later than other members of the structure, this defect is one of the weaknesses of this model. One of the advantages of this model is the geometry of the damper and its location. After drifting, the frames of these dampers slipped on each other without any twisting, and friction was created on their members. It should be noted that in this study all displacements are expressed in terms of drift ratio, which is a dimensionless parameter obtained by dividing the lateral displacement of the frame by the column height (1000 mm).

Figure 6c displays the model's failure at the end of the loading (drift 0.06). It indicates severe damage to the left column and cracks at the beginning and end of the right column, while the beam remains intact. One disadvantage of this model is that the column shortens due to the placement of two brace members at the top and bottom. The column shortening has also changed the frame's behavior. Subsequently, a two-line diagram representing the seismic parameters of the frame is drawn and presented in Figure 6d. Figure 7a indicates the hysteresis diagram of the M2 model. In this case, the primary rings of the hysteresis are thin and irregular. In drift 0.02, the first drop in the diagram was observed, and the experiment in drift 0.06 ended with damper distortion and beam failure in the connection to the damper. In this model, it can be observed that with frame drift, sliding occurs with difficulty. During the 0.02 drift, the plates showed distortion (as seen in Figure 7b). The damper's improper sliding mechanism caused significant damage to the middle of the beam in the final moment (as illustrated in Figure 7c).

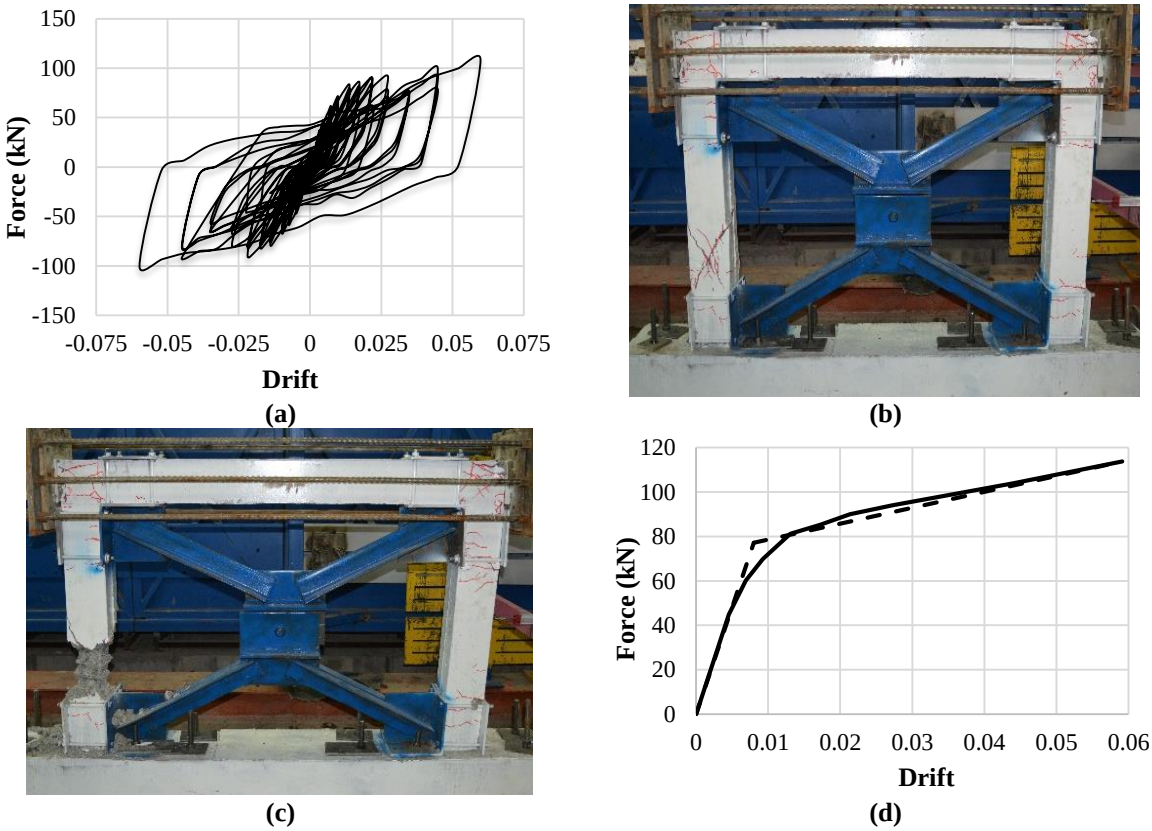

Fig. 6. The results of the M1 sample: a) The hysteresis diagram; b) Condition of the frame at the beginning of yielding; c) Condition of the frame at the end of loading; and d) The equivalent bilinear diagram

The hysteresis diagram of the M3 model is illustrated in Figure 8a. In this instance, the hysteresis loops are more uniform and broader than those of the previous models. Until the final moment, corresponding to a drift ratio of 0.08, no degradation was observed in the hysteresis diagram.

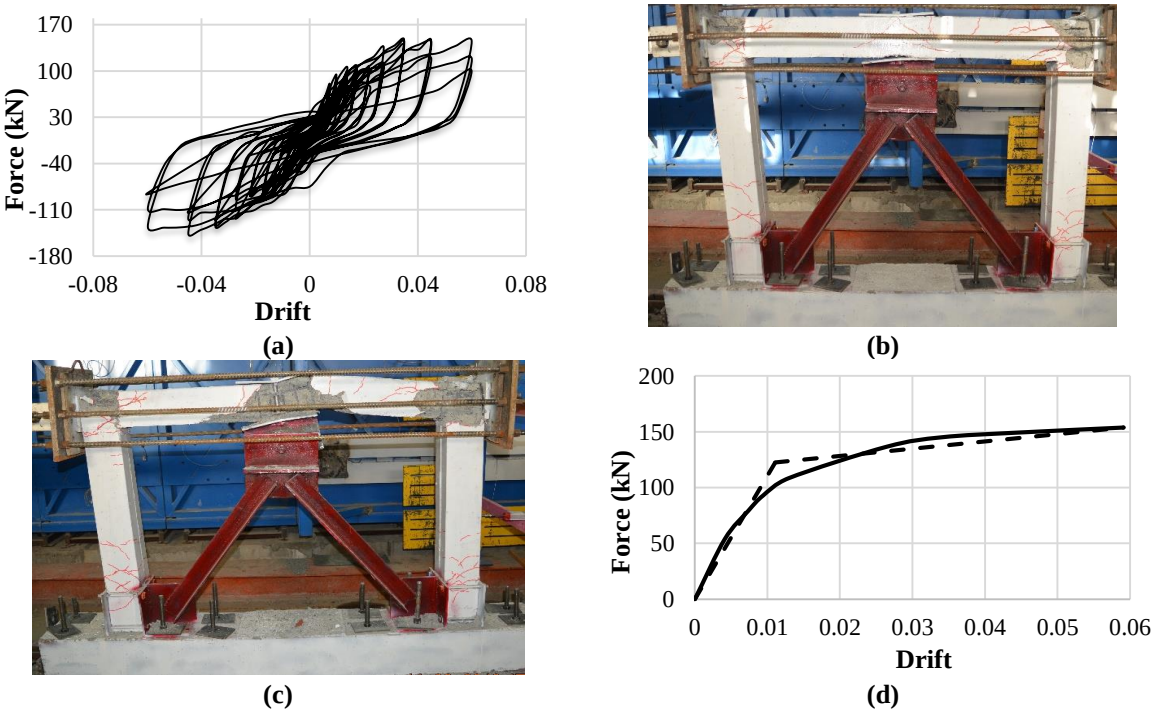

Fig. 7. a) Hysteresis diagram; b) Frame condition at the beginning of yielding; c) Frame condition at the end of loading; and d) Equivalent bilinear diagram of M2 sample

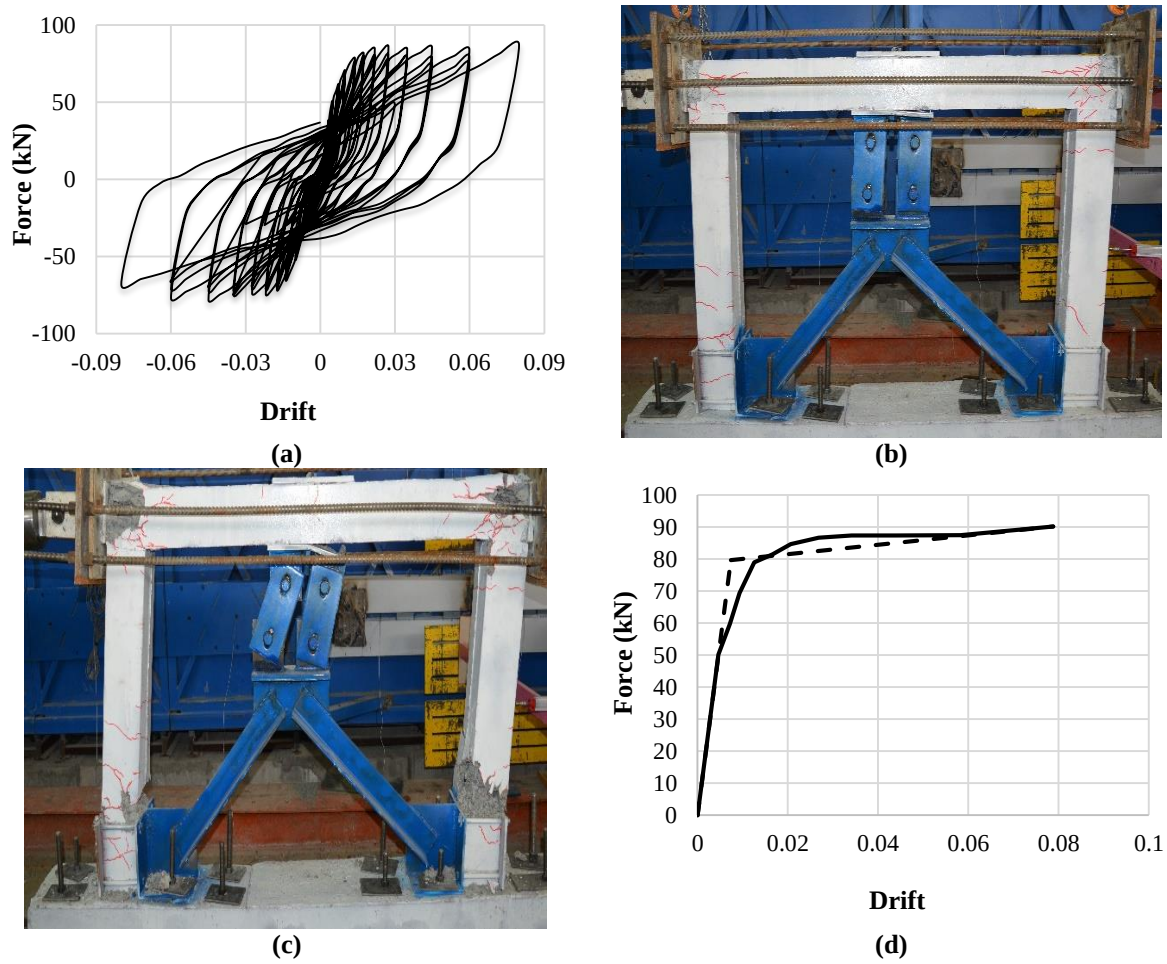

Fig. 8. a) Hysteresis diagram; b) Frame condition at yielding; c) Frame condition at loading end; and d) Bilinear diagram of M3 sample

One significant advantage of this damper is its effective performance; during frame drift ratio, the plates slide over each other smoothly without causing any distortion. Due to the limitations of the loading system, a load of 0.08 was applied, as shown in Figure 8c, at the final loading moment, with its corresponding bilinear diagram depicted in Figure 8d. Figure 9 illustrates the comparison between the seismic parameters of three concrete moment-resisting frames equipped with friction dampers and bare frames. These parameters are derived from bilinear diagrams and hysteresis loops. The results include ductility, calculated using Eq. (2), and elastic stiffness, determined by Eq. (1).

Additional results encompass strength and cumulative energy dissipation, which correspond to the maximum tolerable force of the frame and the enclosed area within the hysteresis loops, respectively. As depicted, the M3 model demonstrates superior performance in terms of ductility (Figure 9a), with ductility approximately twice that of the other models. Conversely, the M2 model shows poor performance in this parameter, with ductility nearly equivalent to that of the bare frame.

Regarding elastic stiffness (Figure 9b), similar to ductility, the M3 model outperforms the other models, with stiffness being 1.5 and 1.3 times greater than those of M2 and M1, respectively. Regarding the frame strength parameter (Figure 9c), the M2 model performed better than the other two. The M3 model exhibited weaker performance compared to the other samples. Figure 9d illustrates the energy dissipation of the models, which corresponds to the enclosed area within the hysteresis loops. It can be seen that in this parameter, the best performance is related to M3, followed by the M2 model.

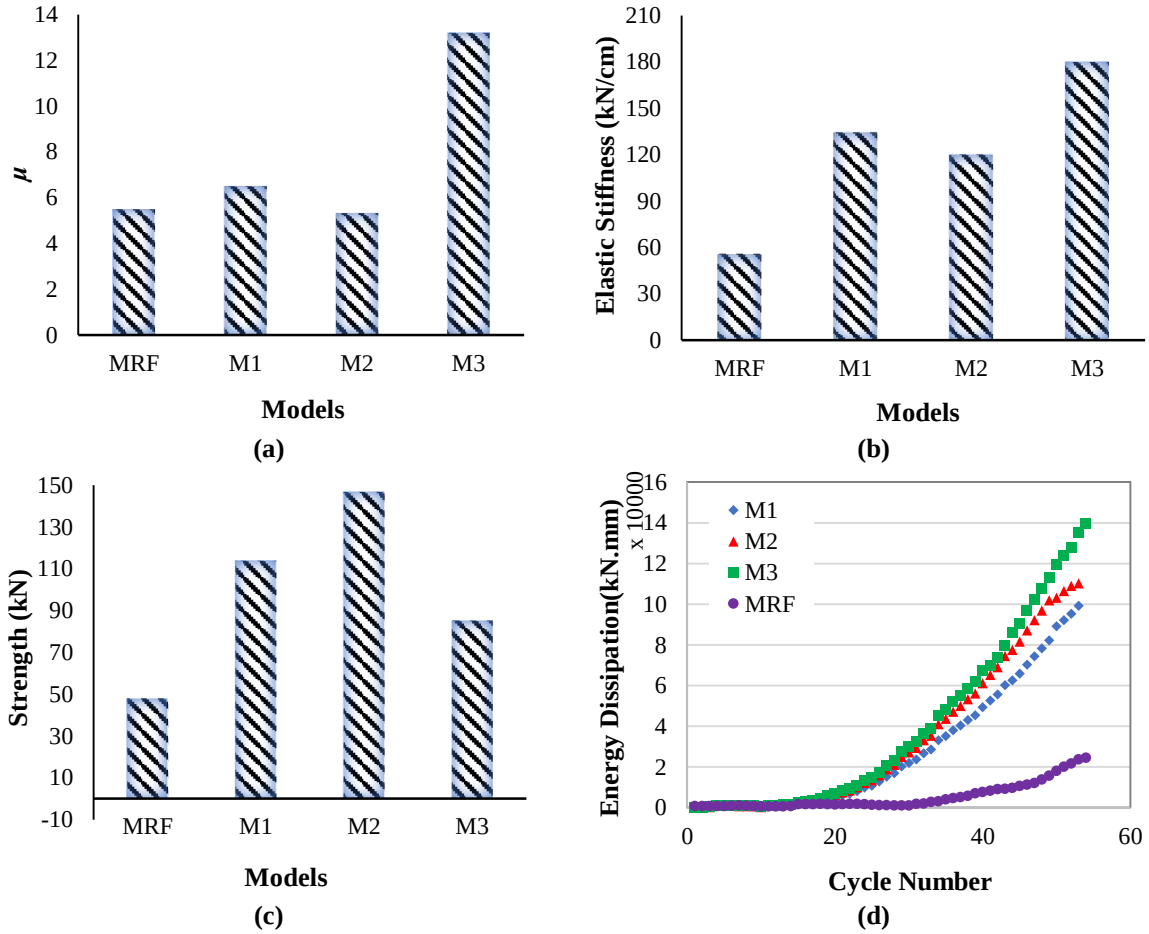

Fig. 9. The results: a) Ductility; b) Elastic stiffness; c) Strength; and d) Energy dissipation of the samples

Another significant conclusion that can be drawn from Figure 9 is that the most substantial impact of adding a damper to the frame is energy dissipation. For instance, in terms of energy dissipation, the M2 model was 5 times greater, and the M1 and M3 models were 4.7 and 6.36 times greater, respectively, than the bare frame model. It can be concluded that the best performance, based on experimental evidence and parameter results, belongs to the M3 model, whose ductility, energy dissipation, stiffness, and strength are 2.4, 6.36, 3.2, and 1.8 times greater, respectively, than those of the bare frame.

3. Parametric Study

3.1. Calculation of Damper Sliding Force

In the experimental specimens, the frames were equipped with dampers of various geometries. Since the sliding force significantly affects the seismic behavior of the frame, numerical studies were conducted in this section. The numerical model chosen for investigation in this part was M3, which exhibited superior behavior compared to other models. The numerical models in this section were analyzed using ABAQUS software. Initially, numerical studies were conducted to calculate the sliding force of the friction damper.

Accordingly, the friction damper, simulated with solid elements, was modeled as shown in Figure 10. By applying displacements, the sliding force of the damper was computed. The analysis type considered was non-linear static. To enhance the numerical model accuracy, large deformations were considered in the analysis (Cheraghi et al., 2023). This figure depicts essential parameters of the damper, such as the pretension force of the bolts, the vertical distance between bolts, and the friction coefficient between plates. After extensive numerical studies, an

approximate Eq. (3) for the sliding force of the friction damper was obtained.

These approximate equations, according to the curve fitting technique, have been presented for the results of numerical models in many studies. The advantage of these equations is the faster estimation of results with acceptable accuracy. In this equation, N, h, μ, and r represent the prestressing force of the bolts, the vertical distance between the bolts, the friction coefficient, and the number of vertical links, respectively.

$$F_s = \frac{4.065 r N^{1.02} \mu^{0.995}}{h^{0.9}} \quad (3)$$

The proper utilization of Eq. (3) necessitates consideration of the following significant notes:

- The coefficient of friction between the bolts and the plate was assumed to be the same as the friction between the plates.
- The rotation of the upper and lower sections of the damper, specifically the parts connected to the beam and the braces, was restricted. Similarly, this equation is presented for these boundary conditions.
- The force and height units are "kN" and "cm", respectively.

To ensure the accuracy of the approximate Eq. (3) results, ten numerical models of dampers with varying dimensions were defined, as shown in Table 3. The sliding force of the damper was then calculated numerically and approximately, with the results shown in Figure 11. As can be seen, the results are close to each other and have acceptable accuracy.

3.2. Numerical Analysis of Concrete Frame Equipped with Friction Damper

In designing and simulating the M3 model, the following points should be considered:

- The damper should be located in a part of the structure that experiences the most drift ratio.
- If the damper sliding force (the force that causes the damper to start sliding) is high, the frame acts like a braced frame, and the main frame members break before the damper slips. If the sliding force is small, its effect on the frame is negligible. Therefore, the optimal sliding force can be calculated.
- The sliding force of the damper depends on the strength of the bare frame.

As the strength of the bare frame increases, the sliding force of the damper must also increase. Therefore, one of the critical aspects of designing these dampers is the calculation of the sliding force to achieve optimal frame performance. The frame of the experimental model was modeled with the same scale of 1:3, i.e., the length of the column and the beam are 1 m and 1.45 m, respectively (Figure 14a). The dimensions of the beam and column sections, rebars, and their final and yield stresses are shown in Tables 1 and 2. The experimental sample was simulated using the elements presented in Table 4 in ABAQUS.

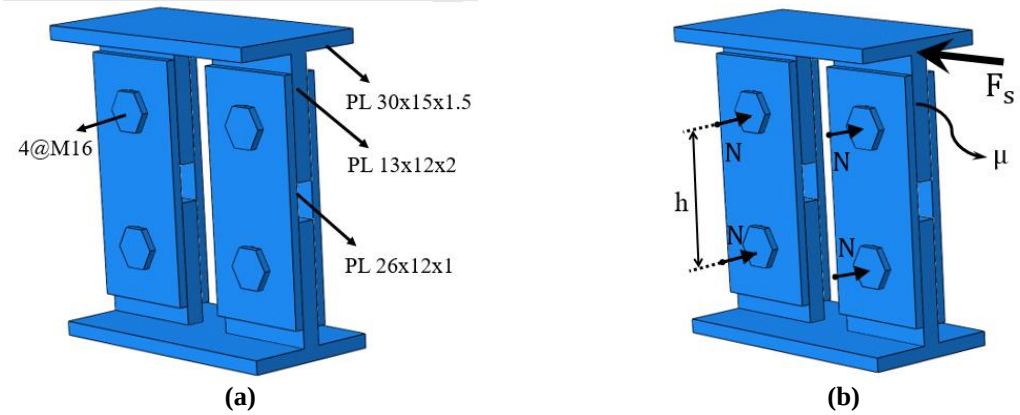

(a) **(b)**

Fig. 10. a) Dimensions of the friction damper (units cm); and b) Introduction of the damper parameters

Table 3. Models for validating Eq. (3)

Models	H (cm)	N (kN)	μ
1	14.5	140	0.2
2	25	80	0.2
3	30	40	0.8
4	14.5	20	0.8
5	14.5	50	0.6
6	30	80	0.6
7	30	120	0.6
8	25	40	0.8
9	30	40	0.2
10	25	120	0.2

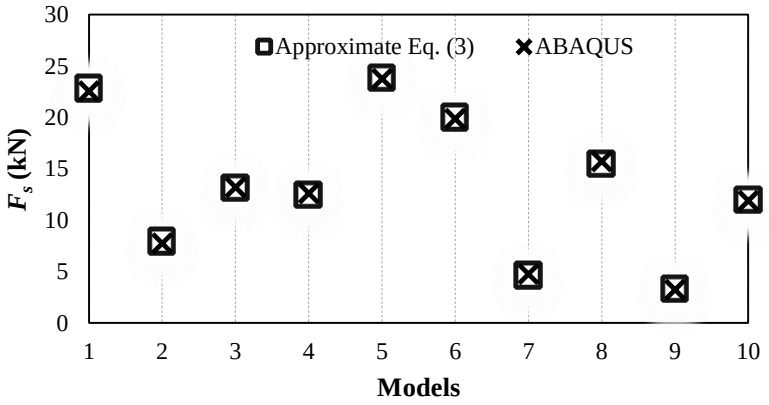

Fig. 11. Comparison of damper sliding force results from numerical analysis and Eq. (3)

Table 4. The type and dimensions of the element used in the numerical model

Parts	Type of element	Mesh dimensions (cm)
Concrete	C3D8R	3 × 3 × 3
Rebar	B31	5
Braces	C3D8R	4 × 4 × 4
Connection plates	C3D8R	4 × 4 × 4
Friction plates	C3D8R	1 × 1 × 1
Bolts	C3D8R	0.5 × 0.5 × 0.5

The mesh dimensions, also shown in this table, were determined based on sensitivity analyses. The analysis in this section involved a static nonlinear analysis using the displacement-control method. Since there was no slippage between the steel and concrete members in the experimental sample, these connections were simulated as "Tie" constraints in the numerical model.

Due to the sensitivity of the model to the behavior of the bolts, their mesh size was considered as small as possible. The concrete damage behavior was selected based on the Concrete Damaged Plasticity (CDP) in the numerical model. This behavioral model has the ability to simulate concrete under complex loads and concrete rupture mechanisms. Table 5 lists the parameters used in the ABAQUS software for this model (Pijpers and Slot, 2020). Fb_0 / fc_0 denotes the ratio of the initial equibiaxial (Equal strength in two directions) compressive yield stress to the initial uniaxial compressive yield stress, and K represents the ratio of the second stress invariant on the tensile meridian.

Initially, the experimental model M3 was calibrated. Figure 12a depicts the simulation of a numerical model with the same dimensions and characteristics as the experimental sample. The diameter of the bolts was 1.6 cm, and their vertical distance was 14.5 cm. The pre-tensioning force of the bolts was defined as the force applied in the experiment, measured by a torque meter, and its friction coefficient was considered 0.6. Figure 14b shows the mesh model of the model, and Figure 14c shows the stress contour of the model after loading. Additionally, the following assumptions were made in the numerical modeling:

• Slips between concrete and rebars were neglected.

• In the experimental sample, no cracking was observed in the foundation until the end of loading. Furthermore, the rotation at the base of the column remained almost zero until the end of loading. Therefore, the foundation was not included in the numerical model.

The analysis was performed in two non-linear static steps. In the first step, the prestressing force of the bolts was applied, and in the second step, the lateral displacement was applied.

After analysing the numerical model, the force-displacement diagram was compared with the backbone diagram of the experimental model shown in Figure 12d. As can be seen, the numerical model provides acceptable results. To investigate the impact of damper sliding force on the seismic performance of a concrete frame, 7 numerical analyses were performed. The damper sliding force varied according to Table 6, which shows the details of the friction damper used in the model. The damper sliding force in these models was calculated using Eq. (3).

After analyzing the models presented in Table 6, the force-displacement diagram for each model was computed, and its bilinear diagram was also extracted. Then, seismic parameters, including elastic stiffness, ultimate strength, ductility, and energy dissipation (area under the force-displacement diagram), were calculated. The results of these analyses are shown in Figure 13. The ductility of the models with respect to the damper sliding force is illustrated in Figure 13a. As can be seen, the model with a damper sliding force of 47.7 kN yielded the best results. The energy absorption results in Figure 13b show the same result. As the damper sliding force increases, both of these results have decreased. The high damper sliding force in these models has caused the primary structural members to yield prematurely.

Table 5. CDP parameters

Dilation angel	Eccentricity	Fb_0 / fc_0	K	Viscosity parameter
34	0.1	1.16	0.667	0.001

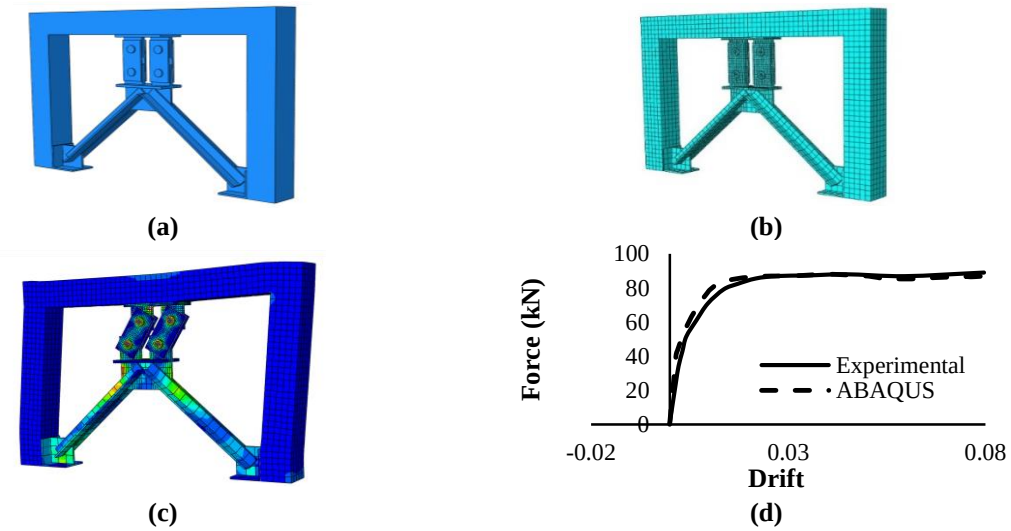

Fig. 12. a) Numerical model,; b) Meshed model; c) Stress contour of the model after loading; and d) Comparison of numerical and experimental results

Table 6. Specifications of numerical analyses

μ	h (cm)	N (kN)	F_s (kN)
0.6	14.5	40	18.8
0.6	14.5	60	28.3
0.6	14.5	80	38
0.6	14.5	100	47.7
0.6	14.5	120	57.6
0.6	14.5	140	67.5
0.6	14.5	160	77.6

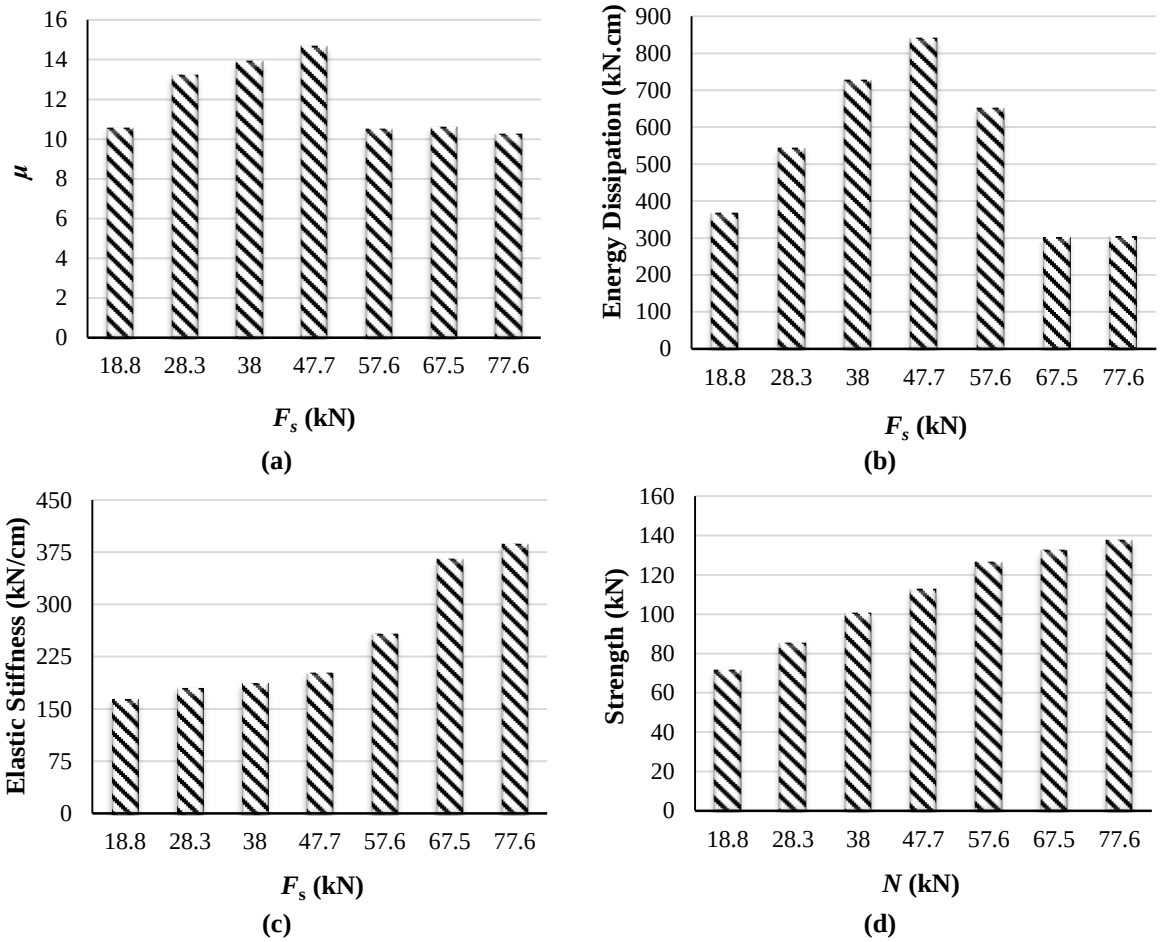

Fig. 13. Results: a) Ductility; b) Energy dissipation; c) Elastic stiffness; and d) Strength

The elastic stiffness of the models is shown in Figure 13c. It can be seen that with the increase in damper sliding force, the stiffness of the models also increases. The slope of the stiffness increase of the frame is not significant until the damper sliding force reaches 47.7 kN; however, beyond this point, the slope increases further. Finally, the final strength of the models is shown in Figure 13d. As the damper sliding force increases, the ultimate strength also experiences an almost linear increase. This increase in the frame's strength is nearly equal to the increase in the sliding force of the damper. That is, the ultimate strength of the frame is equal to the sum of the strength of the bare frame and the sliding force of the damper. Figure 1c shows that the bare frame has a strength of 34 kN. In terms of ductility and energy dissipation, the frame performed best under a specific sliding force. Similarly, if the sliding force of the damper is 1.4 times the strength of the bare frame, the frame will exhibit the best ductility and energy dissipation behavior. With this technique, the results can be extended to other frames.

4. Conclusions

This study investigates the seismic performance of RC frames equipped with friction dampers. To achieve this, three 1:3 scale RC frames were constructed and equipped with friction dampers. The experimental samples were subjected to cyclic loading, and their performance was evaluated using hysteresis curves and other experimental observations. Two samples, M1 and M2, were equipped with dampers exhibiting translational behavior, whereas the third specimen (M3) demonstrated rotational behavior. Subsequently, parametric studies were conducted to investigate the impact of bolt pretension force on the behavior of the frame. The

studies focused on model M3, which exhibited superior performance compared to the other models. In this section, an approximate equation based on curve fitting was proposed for the damper sliding force.

Finally, the effect of the slip force of the damper on the seismic behavior of the RC frame was investigated through nonlinear static analyses. The outputs of the numerical model included ductility, stiffness, strength, and energy dissipation. The summary of the results of this study is presented in the following points:

- The results of the experimental samples showed that rotational friction dampers perform better than translational dampers. Additionally, the hysteresis loops of the frames equipped with rotational friction dampers were fatter and more regular compared to the other two models.
- Experimental results demonstrated that equipping a concrete frame with rotational friction dampers increases energy dissipation, ductility, stiffness, and strength by 6.36, 2.4, 3.2, and 1.8, respectively, compared to a bare frame.
- The approximate equation proposed for calculating the slip force of rotational friction dampers showed good agreement with numerical results. According to this equation, considering the pre-tension force of bolts, vertical bolt spacing, friction coefficient, and the number of vertical links, the slip force of the damper can be easily estimated.
- Numerical studies on the seismic performance of concrete frames equipped with rotation dampers showed that increasing the slip force of the dampers enhanced the stiffness and lateral strength of the frame. The increase in frame strength is approximately proportional to the increase in slip force of the dampers.

Results regarding ductility and energy dissipation of frames equipped with rotation friction dampers demonstrated that the best performance is achieved when the slip force of the dampers is 1.4 times that of the bare frame.

5. Declaration

Artificial intelligence was used only for checking and improving the grammar of the manuscript. No AI tools were used for data analysis, interpretation of results, or generation of scientific content.

6. References

Aghani, H., Cheraghi, K. and Bakhshipour, M. (2024). "Numerical investigation of the effect of aluminum yielding damper for the retrofitting of semi-rigid steel frames", *Periodica Polytechnica Civil Engineering*, 68(2), 349-357, https://doi.org/10.3311/PPci.23119.

Aydin, E., Öztürk, B. and Dutkiewicz, M. (2019). "Analysis of efficiency of passive dampers in multistorey buildings", *Journal of Sound and Vibration*, 439, 17-28, https://doi.org/10.1016/j.jsv.2018.09.031.

Aydin, E., Öztürk, B., Kebeli, Y.E. and Gültepe, G. (2023). "An experimental study on the effects of different pendulum damper designs on structural behavior", *Seismic Isolation, Energy Dissipation and Active Vibration Control of Structures, WCSI 2022, Lecture Notes in Civil Engineering*, 309, 240-253, https://doi.org/10.1007/978-3-031-21187-4_18.

Bruschi, E. and Quaglini, V. (2022). "Assessment of a novel hysteretic friction damper for the seismic retrofit of reinforced concrete frame structures", *Structures*, 46, 793-811, https://doi.org/10.1016/j.istruc.2022.10.113.

Cheraghi, K. and TahamouliRoudsari, M. (2024). "Analytical and numerical investigation of the cyclic behavior of angled u-shape damper", *Steel and Composite Structures*, 51(3), 325-335, https://doi.org/10.12989/scs.2024.51.3.325.

Cheraghi, K., TahamouliRoudsari, M. and Kiasat, S. (2023). "Numerical and analytical investigation of u-shape dampers and its effect on steel frames", *Structures*, 55, 498-509, https://doi.org/10.1016/j.istruc.2023.06.037.

Cheraghi, K., TahamouliRoudsari, M., Kiasat, S. and Cheraghi, K. (2024). "Numerical and analytical investigation of cyclic behavior of D-shape yielding damper", *Structural Engineering and Mechanics*, 89(4), 411-420, https://doi.org/10.12989/sem.2024.89.4.411.

American Concrete Institute (ACI) Committee 374 (2005). *ACI COD-374.1-05(19): Acceptance criteria for moment frames based on structural testing and commentary*, ACI, 374, 1-05, https://www.concrete.org/store/productdetail.aspx?ItemID=374105.

Building Seismic Safety Council (BSSC) (2006). *NEHRP recommended provisions: design*

examples, US Department of Homeland Security, Federal Emergency Management Agency, FEMA 451, https://www.scribd.com/document/66637013/FEMA-451-NEHRP-Design-Examples-2006.

Federal Emergency Management Agency (FEMA). (2000). *Prestandard and commentary for the seismic rehabilitation of buildings*, Report FEMA-356, Washington, DC.

Ganjimorad, S., Permanoon, A. and Azadi, M. (2024). "Analyzing lateral strength and failure modes in masonry infill frames: A mesoscale study", *Earthquakes and Structures*, 27(2), 113-126, https://doi.org/10.12989/eas.2024.27.2.113.

Gao, J., Wang, C.L., Meng, S. and Zeng, B. (2023). "Performance evaluation of friction dampers considering different metal pairs and loading rates", *Journal of Constructional Steel Research*, 204, 107859, https://doi.org/10.1016/j.jcsr.2023.107859.

Hu, S., Qiu, C. and Zhu, S. (2023). "Floor acceleration control of self-centering braced frames using viscous dampers", *Journal of Building Engineering*, 74, 105944, https://doi.org/10.1016/j.jobe.2023.105944.

Huang, L., Clayton, P.M. and Zhou, Z. (2021). "Seismic design and performance of self-centering precast concrete frames with variable friction dampers", *Engineering Structures*, 245, 112863, https://doi.org/10.1016/j.engstruct.2021.112863

British Standards Institution (2009). *BS EN ISO 898-1:2009- Mechanical properties of fasteners made of carbon steel and alloy steel-part 1: bolts, screws and studs with specified property classes-coarse thread and fine pitch thread*, London: British Standards Institution https://fpg-co.com/Standards/ISO898-1.pdf.

Javaheri-Tafti, M. and Hajisafari, M. (2025). "Comparison of conventional and energy method in evaluating the seismic fragility of reinforced concrete frames", *Civil Engineering Infrastructures Journal*, 58(1), 71-86, https://doi.org/10.22059/ceij.2024.360893.1928

Kim, J. and An, S. (2016). "Optimal distribution of friction dampers for seismic retrofit of a reinforced concrete moment frame", *Advances in Structural Engineering*, 20(10), 1523-1539, https://doi.org/10.1177/1369433216683197.

Liu, Y., Zhou, W. and Xie, X. (2023). "Experimental study of precast self-centering concrete shear walls with external friction dampers", *Journal of Building Engineering*, 68, 106182, https://doi.org/10.1016/j.jobe.2023.106182.

Maida, Y. and Sakata, H. (2021). "Cyclic loading test of reinforced concrete frames protected with brace-type friction dampers", *Advances in Structural Engineering*, 25(1), 83-97, https://doi.org/10.1177/13694332211042785.

Moon, K.H., Han, S.W. and Lee, C.S. (2017). "Seismic retrofit design method using friction damping systems for old low and mid-rise regular reinforced concrete buildings", *Engineering Structures*, 146, 105-117, https://doi.org/10.1016/j.engstruct.2017.05.031.

Morgen, B.G. and Kurama, Y.C. (2008). "Seismic response evaluation of posttensioned precast concrete frames with friction dampers", *Journal of Structural Engineering*, 134(1), 132-145, https://doi.org/10.1061/(ASCE)0733-9445(2008)134:1(132).

Nabid, N., Hajirasouliha, I., Escolano Margarit, D. and Petkovski, M. (2020). "Optimum energy based seismic design of friction dampers in RC structures", *Structures*, 27, 2550-2562, https://doi.org/10.1016/j.istruc.2020.08.052.

Ozturk, B., Cetin, H. and Aydin, E. (2022). "Optimum vertical location and design of multiple tuned mass dampers under seismic excitations", *Structures*, 41, 1141-1163, https://doi.org/10.1016/j.istruc.2022.05.014.

Permanoon, A., Pouraminian, M., Khorami, N., Ganjimorad, S., Azarkhosh, H., Sadrinejad, I. and Pourbakhshian, S. (2024). "Improving mixed-mode fracture properties of concrete reinforced with macrosynthetic plastic fibers: an experimental and numerical investigation", *Buildings*, 14(8), 2543, https://doi.org/10.3390/buildings14082543.

Pijpers, R.J.M. and Slot, H.M. (2020). "Friction coefficients for steel to steel contact surfaces in air and seawater", *Journal of Physics: Conference Series*, 1669(1), 012002, https://doi.org/10.1088/1742-6596/1669/1/012002.

Rahimi, H., Esfandiari, J. and Tahamouliroudsari, M. (2022). "Experimental and numerical study using NSD metal damper has been used in concrete moment frames", *Amirkabir Journal of Civil Engineering*, 54(9), 3353-3372, https://doi.org/10.22060/ceej.2022.20435.7426.

Roodpeyma, A.H. and Mahmoudzadeh Kani, I. (2023). "Evaluation of seismic designed pipe racks under accidental explosions with finite element method", *Civil Engineering Infrastructures Journal*, 56(1), 105-116, https://doi.org/10.22059/ceij.2022.328868.1794